

RESEARCH

Open Access



Anti-HIV reverse transcriptase plant polyphenolic natural products with in silico inhibitory properties on seven non-structural proteins vital in SARS-CoV-2 pathogenesis

Von Novi O. de Leon^{1,2}, Joe Anthony H. Manzano^{1,2}, Delfin Yñigo H. Pilapil IV^{1,2}, Rey Arturo T. Fernandez¹, James Kyle Anthony R. Ching^{1,3}, Mark Tristan J. Quimque^{1,4,5}, Jay Carl M. Agbay^{5,6}, Kin Israel R. Notarte⁷ and Allan Patrick G. Macabeo^{1*}

Abstract

Background: Accessing COVID-19 vaccines is a challenge despite successful clinical trials. This burdens the COVID-19 treatment gap, thereby requiring accelerated discovery of anti-SARS-CoV-2 agents. This study explored the potential of anti-HIV reverse transcriptase (RT) phytochemicals as inhibitors of SARS-CoV-2 non-structural proteins (nsps) by targeting in silico key sites in the structures of SARS-CoV-2 nsps. One hundred four anti-HIV phytochemicals were subjected to molecular docking with nsp3, 5, 10, 12, 13, 15, and 16. Top compounds in complex with the nsps were investigated further through molecular dynamics. The drug-likeness and ADME (absorption, distribution, metabolism, and excretion) properties of the top compounds were also predicted using SwissADME. Their toxicity was likewise determined using OSIRIS Property Explorer.

Results: Among the top-scoring compounds, the polyphenolic functionalized natural products comprised of biflavones **1**, **4**, **11**, **13**, **14**, **15**; ellagitannin **9**; and bisisoquinoline alkaloid **19** were multi-targeting and exhibited strongest binding affinities to at least two nsps (binding energy = -7.7 to -10.8 kcal/mol). The top ligands were stable in complex with their target nsps as determined by molecular dynamics. Several top-binding compounds were computationally druggable, showed good gastrointestinal absorptive property, and were also predicted to be non-toxic.

Conclusions: Twenty anti-HIV RT phytochemicals showed multi-targeting inhibitory potential against SARS-CoV-2 non-structural proteins 3, 5, 10, 12, 13, 15, and 16. Our results highlight the importance of polyhydroxylated aromatic substructures for effective attachment in the binding/catalytic sites of nsps involved in post-translational mechanism pathways. As such with the nsps playing vital roles in viral pathogenesis, our findings provide inspiration for the design and discovery of novel anti-COVID-19 drug prototypes.

Keywords: SARS-CoV-2, Non-structural proteins, Molecular docking, ADMET, Polyphenolics, Terpenoids, Alkaloid, HIV reverse transcriptase

* Correspondence: agmacabeo@ust.edu.ph

¹Laboratory for Organic Reactivity, Discovery and Synthesis (LORDS), Research Center for the Natural and Applied Sciences, University of Santo Tomas, España Blvd., 1015 Manila, Philippines
Full list of author information is available at the end of the article



© The Author(s). 2021 **Open Access** This article is licensed under a Creative Commons Attribution 4.0 International License, which permits use, sharing, adaptation, distribution and reproduction in any medium or format, as long as you give appropriate credit to the original author(s) and the source, provide a link to the Creative Commons licence, and indicate if changes were made. The images or other third party material in this article are included in the article's Creative Commons licence, unless indicated otherwise in a credit line to the material. If material is not included in the article's Creative Commons licence and your intended use is not permitted by statutory regulation or exceeds the permitted use, you will need to obtain permission directly from the copyright holder. To view a copy of this licence, visit <http://creativecommons.org/licenses/by/4.0/>.

Background

The rapid spread of the severe acute respiratory syndrome coronavirus 2 (SARS-CoV-2) marks itself as one of the deadliest viruses in recent history due to its high mortality and morbidity rates [1, 2]. As of May 2021, the World Health Organization recorded over one hundred sixty-seven million cases worldwide with 3.4 million deaths [3]. Continuous efforts are being carried out to unravel the pathophysiology of the virus, paving the way to the discovery and development of efficacious vaccines and anti-SARS-CoV-2 drugs. While the world continues to make strides in vaccine development and rollout, drug-based treatments are still needed to cure the growing number of COVID-19-afflicted individuals. Thus, developing effective therapeutic agents against SARS-CoV-2 remains a global health need.

The discovery of antiviral chemotherapeutic prototypes requires accurate identification of drug targets. Among which, the SARS-CoV-2 non-structural proteins (nsps) are among the highly favored targets because of their role in viral replication, post-translational mechanisms, and host immunity evasion that influence SARS-CoV-2 virulence and pathogenesis [4]. The repurposing of bioactive natural products is one of the key strategies available for screening potential SARS-CoV-2 nsps inhibitors. To date, plant-based medicines as treatment for SARS-CoV-2 infection have not been reported.

Plant-derived natural products are established biotechnological-derived substances that exhibit a wide range of biological activity including antagonistic properties against human immunodeficiency virus (HIV) and coronaviruses such as Middle East respiratory syndrome coronavirus (MERS-CoV) and SARS-CoV [5–9]. Relevant to this study, polyphenolic natural products such as flavonoids and tannins (Fig. 1) are well-recognized to confer broad-spectrum antiviral activities in addition to possessing anti-inflammatory, anti-tumor, antioxidants, immune, and prebiotic properties [10]. Recent studies in anti-COVID-19 drug discovery have highlighted the potential of polyphenolic compounds through in silico-guided investigations against protein targets in SARS-CoV-2 involved in infective mechanisms, i.e., inhibition of spike (*S*) protein, angiotensin-converting enzyme 2 (ACE-2) receptor, papain-like protease (PLpro), 3-chymotrypsin-like cysteine protease (3CLpro), and RNA-dependent-RNA-polymerase (RdRp) [10–13]. In addition, computational studies describing the potential of other classes of natural products as SARS-CoV-2 3CLpro, PLpro, and RdRp protein inhibitors have been reported [5, 14–19].

Considering the similarity between SARS-CoV-2 and HIV, we repurposed previously reported anti-HIV reverse transcriptase (RT) secondary compounds using in silico simulations in this study. SARS-CoV-2 and HIV

are single-stranded RNA viruses that utilize RNA-dependent polymerases and code precursor polyproteins vital for their respective pathogenesis. In this paper, we disclose computational interrogation of 104 known anti-HIV RT phytochemicals against seven target proteins, namely nsp3 (PLpro), nsp5 (3CLpro), nsp12 (RdRp), nsp13 (helicase), nsp15 (endoribonuclease), and the nsp16-nsp10 complex (*S*-adenosylmethionine complex). The thermodynamic stability and the pharmacokinetic characteristics of the top-ranked compounds are also reported.

Methods

Target enzyme preparation

Seven target enzymes with important functions in SARS-CoV-2 infectivity were selected and obtained from the Protein Data Bank (PDB): 3CLpro (PDB ID: 6LU7), PLpro (PDB ID: 6W9C), RdRp (PDB ID: 6M71), helicase (6JYT), nsp16-nsp10 complex (6W4H), and nsp15 (6VWW). These proteins in three-dimensional structures were added to UCSF Chimera 1.14 platform as PDB files [20]. All proteins belong to SARS-CoV-2 except for helicase due to unavailability of nsp13. Thus, helicase model from SARS-CoV-1 which shares 99.8% sequence identity and 100% sequence similarity with that of SARS-CoV-2 was used [21]. Coronavirus helicase domains are distinct compared to other (+)-sense RNA virus domains due to the presence of linkage in a single protein to a binuclear zinc-binding domain at the N-terminus. This domain is composed of 12 conserved cysteine-histidine residues and is a good target in antiviral drug discovery [22–25].

Ligand selection and preparation

A total of 104 plant secondary metabolites (Supplementary Figure 1; Supplementary Table 1) previously reported to inhibit HIV RT [25] were used as ligands targeting the above-mentioned viral proteins. The plant metabolite structures were formatted as SYBYL mol2 file or in SMILES notation using Avogadro (version 1.20) and were added to the UCSF Chimera 1.14 platform [26].

Molecular docking simulations

Molecular docking experiments were carried out on UCSF Chimera 1.14 platform with AutoDock Vina plugged-in as docking algorithm [20]. Protein structures in three dimensions were opened in PDB formats. Co-crystallized ligands and other molecules were removed from the crystallized protein. Ligands were added in the platform as SYBYL mol2 files or in SMILES notation. Ligand and protein structures were minimized through addition of missing hydrogen atoms and charges to the structures using the Gasteiger charge method, which

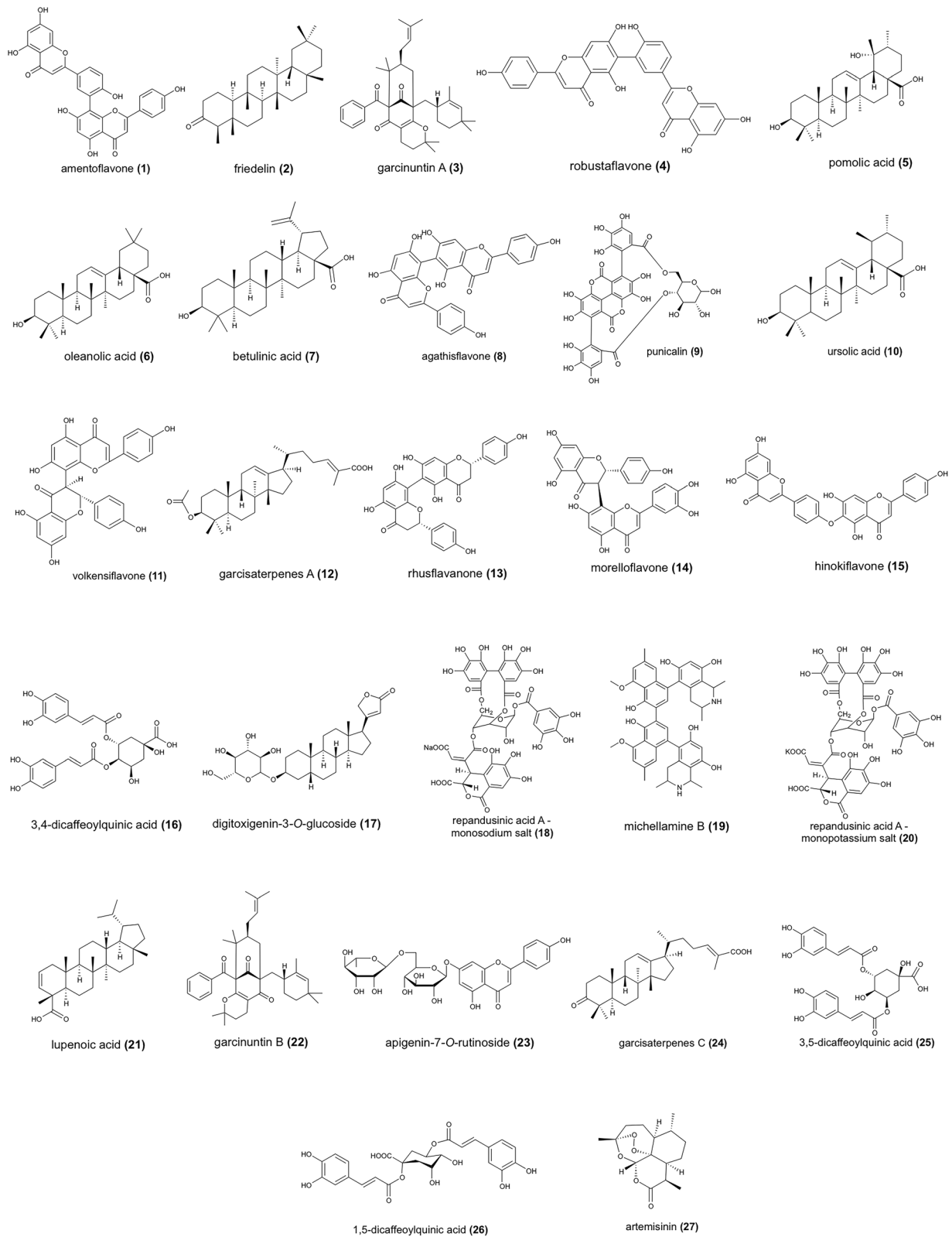


Fig. 1 Anti-HIV RT phytochemicals with strong binding affinities to at least one of the target nsp

was computed using Amber's Antechamber module [27]. 'Flexible ligand into flexible active site' protocol was followed during execution of docking procedures. In this protocol, flexible ligands were allowed and positioned within a grid box (Supplementary Table 2) which encompasses the enzymatic ligand-binding cavity, as predicted using COACH algorithms [28].

Druggability, ADME, and toxicity prediction

Top ten compounds per nsp, which in total were twenty-seven compounds, were selected for druggability, pharmacokinetic, and toxicity analyses. Absorption, distribution, metabolism, and excretion (ADME) properties of top twenty-seven compounds overall were computationally predicted using SwissADME software. Evaluation of pharmacokinetic profiles of compounds was performed according to Lipinski's 'rule of five' which assesses biochemical properties of a drug candidate involved in permeation and cell absorption. Three of the following values need to be met according to Lipinski's criteria: < 500 Daltons (Da) for molecular weight, < 5 for calculated lipophilicity (MLogP), < 10 for the number of hydrogen-bond acceptors, and < 5 for the number of hydrogen bond donors [29]. Moreover, toxicity of hit compounds, specifically mutagenicity, tumorigenicity, reproductive toxicity, and irritant effects, were predicted in silico using OSIRIS Property Explorer software [30]. Solubility (LogS) was also predicted using the same software in which $\text{LogS} \geq -4$ indicates good solubility and favorable absorption of compounds.

Molecular dynamics simulations

Molecular dynamics (MD) simulation was employed to understand the dynamic behavior of the top-binding complexes based on molecular docking analysis. All MD simulations were carried out using GROMACS version 2020.1 under the Ubuntu Linux platform version 2020.1-1 [31]. The SARS-CoV-2 non-structural protein topologies were generated using the CHARMM 36 force field with TIP3P water model, while ligand topology was generated using CGenFF (CHARMM general force field). The complex was solvated on a dodecahedron grid by single point charge (SPC) water. The system was then neutralized with counterions. Energy minimization was done on the system using the steepest descent integrator for 5000 steps and Particle Mesh Ewald (PME) algorithm for the Coulomb and van der Waals interactions [32]. After system equilibration, each system was subjected to molecular dynamic simulation for 20 ns at constant temperature of 300 K. The dynamic trajectories were recorded during the production every 0.01 ns which were used to analyze the root mean square deviation (RMSD) and root mean square fluctuation (RMSF) for each system.

Results

One hundred four repurposed anti-HIV reverse transcriptase phytochemicals against SARS-CoV-2 nsps comprised of polyphenolics, terpenoids, alcohols, and alkaloids were docked with nsps3, 5, 10, 12, 13, 15, and 16. Twenty-seven compounds, which are included in the top 10 compounds per nsp, showed favorable binding affinities (Fig. 1). In addition, twenty of the top compounds exhibited multi-targeting properties.

Molecular docking with autolytic-processing enzymes (nsp3 and nsp5)

Top ten compounds against PLpro exhibited binding affinities of -10.1 to -10.8 kcal/mol (Table 1). The biflavonoid amentoflavone (**1**) exhibited highest affinity to PLpro with its benzopyrone (ring C) and phenolic moiety (ring B) participating through H-bonding (5.62 Å) and *pi*-anion interactions with Lys711, respectively (Fig. 2A). Ring C additionally bound Ile580 through *pi*-alkyl interaction. The phenolic functionality in ring B also participated in hydrogen bonding with His342 (3.49 Å) and in *pi*-alkyl binding with Ala579 and Leu742. Ring A' of the benzopyrone moiety bound Arg712 by H-bonding (5.72 Å) and Ile310 by *pi*-alkyl interaction. Meanwhile, the phenolic moiety (ring B') exhibited *pi*-anion interaction with Asp339 and *pi*-cation interaction with Arg558.

On the other hand, top-ranked ligands against 3CLpro exhibited binding affinities of -7.9 to -8.6 kcal/mol (Table 1). The biflavones amentoflavone (**1**) and volkensiflavone (**11**) showed highest affinity to 3CLpro (Fig. 2B). The chromanone moieties (rings A' and C) of amentoflavone showed stacked amide-*pi* and *pi*-*pi* T-shaped interactions with His41, a component of the 3CLpro catalytic dyad. These interactions were also demonstrated by its phenolic moiety to Asn142. The chromanone moiety (rings A and C) was bound to Met165 through *pi*-alkyl interaction along with hydrogen bonds with Val186 (5.46 Å), Arg188 (5.86 Å), and Glu166 (4.83 Å). Ring A' also bound Cys44 through H-bonding (4.77 Å). Volkensiflavone (**11**) was likewise bound to the 3CLpro catalytic dyad, His41 and Cys145, through *pi*-anion interaction and hydrogen bonding (3.71 Å) of the chromanone moieties (rings C and A' respectively). Moreover, rings A' of the flavone substructure also exhibited hydrogen bonding with Glu166 (3.88 Å) while the B ring residue bound Thr25 through a *pi*-sigma interaction.

Molecular docking with replication-transcription complex enzymes (nsp12 and nsp13)

Among the top ten compounds against RdRp with binding affinities of -8.6 to -9.5 kcal/mol, the ellagitannin punicalin (**9**) exhibited the highest affinity (Table 2; Fig. 3A). The ellagic acid moiety occupied Ile494 and its galloyl hydroxyl bound

Table 1 Binding affinities and interactions of top ten ligands against the cysteine proteases

Target	Cpd	Binding affinity (kcal/mol)	Hydrogen bonds	Other interactions
PLpro	1	-10.8	His342, Lys711, Arg712	Lys711, Asp339, Arg558, Ile310, Ile580, Ala579, Leu742
	2	-10.7	None	His342, Leu557, Ala579, Leu742
	3	-10.7	Lys711, Arg712	Ile310, Ala338, His342, Leu557, Ala579, Ile580, Val635, Lys694, Arg712
	4	-10.6	Thr583, Arg586, Tyr634	Asp339, Arg558, Ala579, Ile580, Met630, Leu742
	5	-10.4	Val659	Leu557, Arg558, Met560, Ala579, Ile580, Leu742
	6	-10.3	Asp226	None
	7	-10.2	Lys711, Arg712	None
	8	-10.2	Asp339, Arg586, Tyr634	Val304, Ala338, Asp339, Arg558, Ala579, Lys711, Leu742
	9	-10.2	Gly337, Asp339, Arg345, Arg558, Arg712	Ile310
	10	-10.1	Asp339, Arg345, Tyr634	Leu557, Ile580, Met630, Val635, Lys711, Leu741
3CLpro	1	-8.6	Cys44, Val186, Arg188, Glu166	Thr25, His41, Asn142, Cys145, Met165
	11	-8.6	Cys145, Glu166	Thr25, His41
	12	-8.5	Thr24, Ser46, Thr190, Gln192	Thr25, His41
	13	-8.5	Thr26, His41	Met49, Pro168
	4	-8.5	Arg188, Gln189	None
	8	-8.4	Thr26, Gln189, Thr190	Leu27, Met49, Glu166, Met165, Pro168
	14	-8.4	Phe140, Gly143, Arg188, Gln189	His41
	15	-8.1	Asn119, Val186	None
	16	-7.9	Gly143, Cys145, Glu166, Gln189	His41, Gln189
	17	-7.9	His41, Asn119	His41, Gly143, His163
	3	-7.9	His41	Leu27, His41

Asn497 (4.13 Å), which are both components of the RdRp finger domain that is responsible for the entry and exit of the RNA template during replication-transcription [33]. Moreover, its glucose hydroxyl and hydrogen participated in hydrogen bonding (4.79 Å) and carbon-hydrogen bonding respectively with Asp684, a component of the motif B of the polymerase active site [34]. Other interactions include the participation of its ellagic acid moiety in *pi*-alkyl interaction with Lys577, galloyl hydroxyl in hydrogen bonding with Gly590 (2.87 Å), carbonyl oxygen in hydrogen bonding with Tyr689 (5.76 Å), and glucose moiety in carbon-hydrogen bonding with Ala685.

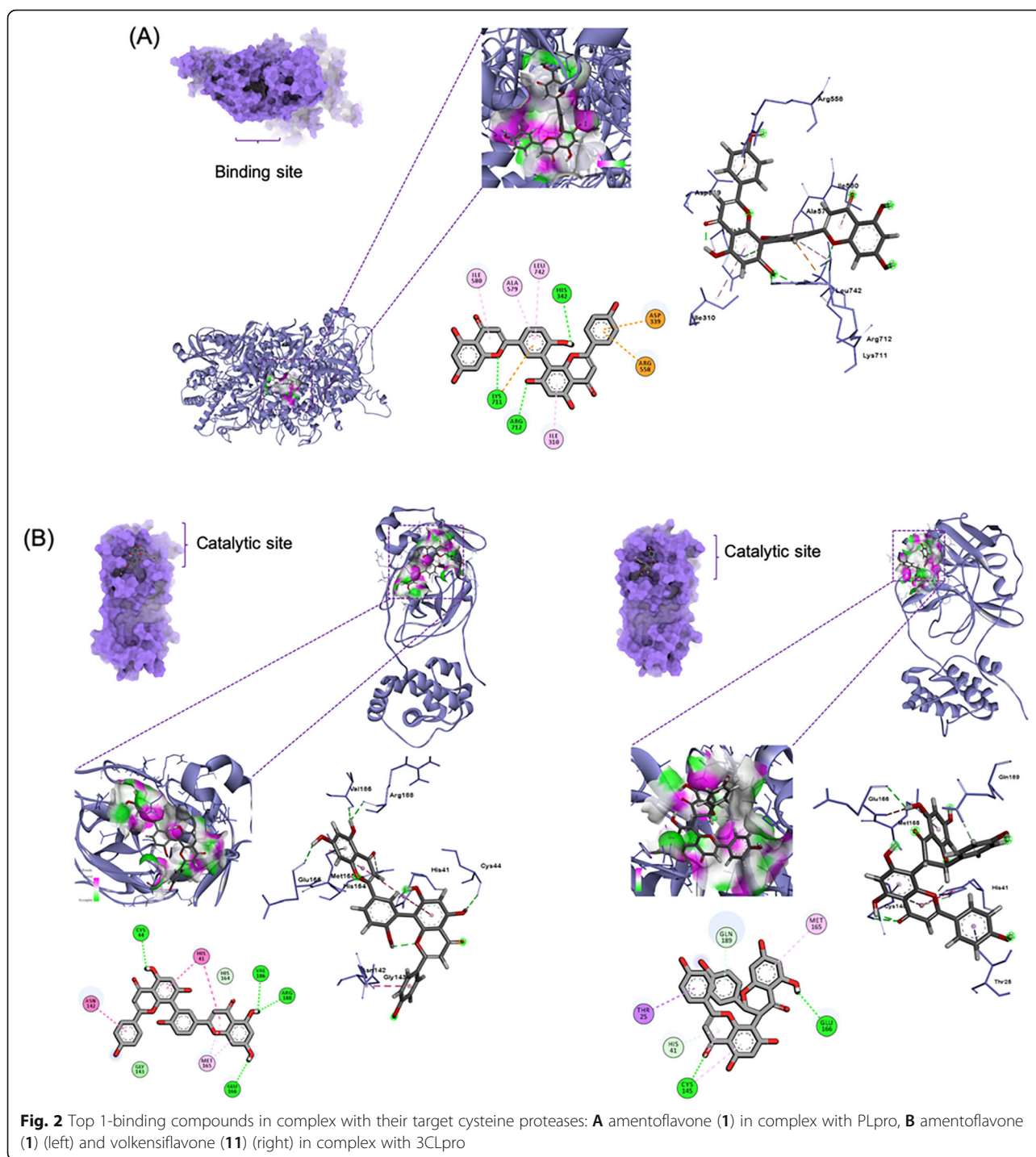
Meanwhile, the top-ranked ligands against helicase had binding affinities of -8.4 to -9.2 kcal/mol in which the biflavonoids rhusflavanone (13) and morelloflavone (14) exhibited the strongest affinity (Fig. 3B). Compound 13 occupied the helicase Rec1A domain, which is a component of the nucleotide binding site, through hydrogen bonding of its chromanone (ring A') hydroxyl and pyrone (ring C') oxygen with Lys288 (4.76 Å) and Ala316 (3.32 Å), respectively [35]; *pi*-alkyl interactions of its chromene moieties, rings A with Ala316 with Ala316, and ring A' with Lys320; and *pi*-cation interaction of its hydroxyphenyl moiety (ring B) with Lys320.

Compound 13 also occupied the Rec2A domain of the nucleotide binding site through a hydrogen bond of its pyrone (ring C) carbonyl with Arg443 (4.73 Å), an amide-*pi* stacked interaction of its hydroxyphenyl moiety (ring B') with Gly538, and a *pi*-sigma interaction of ring B' with Ser539. A pyrone (ring C) carbonyl further contributed to the binding affinity of compound 13 by binding to Thr286 through van der Waals forces. On the other hand, the dihydroxyphenyl moiety (ring B') of compound 14 bound Glu341 through a relatively strong hydrogen bonding (3.02 Å) and both Ala312 and Val340 by *pi*-alkyl interactions. Ring A of its chromanone functionality bound Ala313 through a *pi*-alkyl interaction and also Ala312 by *pi*-sigma interaction. These residues are members of the helicase Rec2A domain of the nucleotide binding site. In addition, a benzophyrone hydroxyl (ring A') of compound 14 bound Asp534 (5.32 Å), which is a residue of the Rec1A helicase domain of the nucleotide binding site.

Molecular docking with enzymes functioning in the evasion of host immunity

SAM-dependent 2'-*O*-methyltransferase complex enzymes (*nsp16-nsp10* complex)

Top compounds against *nsp16* exhibited affinities from -9.3 to -10.6 kcal/mol. The SAM-binding site was



targeted and the biflavonoid robustaflavone (**4**) and the alkaloid michellamine B (**19**) demonstrated the greatest affinity (Table 3; Fig. 4A). Hydroxyphenyl ring B of compound **4** exhibited *pi*-alkyl interactions with Leu6898 and Met6929, and a hydrogen bonding with Cys6913 (3.64 Å). The hydroxyphenyl ring B' showed carbon-hydrogen bonding with Asn6841. Moreover, its benzo-pyrone moiety (rings A and C) was in *pi*-anion

interaction with Asp6897 and its chromene hydrogen was in hydrogen bonding with Asp6928 (3.40 Å). A van der Waals force interaction between its pyrone ring C oxygen and Gly6869 was also observed. Another pyrone moiety (ring C') also interacted with nsp16 through a *pi*-anion interaction with Glu7001. Lys6844 (5.74 Å) and Asn6996 (4.96 Å) were occupied by the pyrone ring C' carbonyl through hydrogen bonding. On the other hand,

Table 2 Binding affinities and interactions of top ten ligands against the nsps vital for replication

Target	Cpd	Binding affinity (kcal/mol)	Hydrogen bonds	Other interactions
RdRp	9	-9.5	Asn497, Gly590, Asp684, Tyr689	Ile494, Lys577, Asp684, Ala685
	10	-9.1	Val495	Ile494, Lys577, Ala580, Ala685
	2	-8.9	None	Ile494, Arg569, Leu576, Lys577, Ala685
	15	-8.9	Asn496, Asn497, Arg569, Ala685	Ile494, Lys500, Lys577, Ala580, Ala685
	18	-8.9	Asn496, Arg569, Ala685, Ser759	Lys545, Arg569
	19	-8.8	Ile548, Lys593, Ser814	Ile548, Lys593, Leu758, Asp761, Cys813, Pro832, Arg836, Ile837, Ala840
	20	-8.8	Ile494, Asp684	Lys500, Lys545, Arg569, Ser682
	4	-8.8	Asn497, Arg569	Ile494, Lys500, Arg569, Lys577, Ala685
	21	-8.7	None	Ile494, Lys500, Leu576, Lys577, Ala685, Tyr689
	1	-8.6	Asn497, Asp684	Arg569, Ala580, Ala688, Tyr689
	3	-8.6	Arg569, Gln573	Ile494, Lys500, Lys577, Ala580, Ile589, Ala685, Ala688, Tyr689
	5	-8.6	Arg569, Gln573	Leu576, Lys577, Ala580, Ala685
	Helicase	14	-9.2	Glu341, Asp534
13		-9.2	Lys288, Ala316, Arg443	Thr286, Ala316, Lys320, Gly538, Ser539
15		-9	Arg332, Glu319, Cys342, Ser310, Asp534	Met378, Ala312, Ala316, Asp315
8		-8.9	Gly285, Ala316, Ser289, Lys288, Glu375, Gln537	Ala312, Lys320, Gln537
4		-8.9	Gly285, Lys288	Arg443, Arg442, Glu540, Lys320, Ala316, Ala312, Ala313
19		-8.7	None	Gly538, Glu319, Glu540, Ala316, Ser535, Ala312, Ala313
1		-8.6	None	Ala312, Cys342, Asp315, Ala316, His311
22		-8.6	Asn459	Phe437, Lys460, Pro434, Gly433, Lys430, Pro402, Tyr457, Ala403
23		-8.5	Lys430, Gln281, Val456, Tyr457	Phe437, Pro434, Lys430, Leu455
24		-8.4	Leu417, Asn557, Asn516	Phe422, Pro406, Pro408

compound **19**'s isoquinoline moiety was in H-bonding with Asp6928 (3.68 Å) and Asp6897 (4.60 Å) and in carbon-hydrogen bonding with Gly6869. Another isoquinoline moiety was in *pi*-anion interaction with Asp6931. Moreover, the naphthalene moiety participated in *pi*-*pi* T-shaped interaction with Phe6947 and in *pi*-sulfur interaction with Cys6914. The methyl group connected to naphthalene manifested alkyl interactions with Met6929, Leu6898, and Cys6913.

In connection, top compounds against nsp10 showed binding affinities of -6.9 to -7.7 kcal/mol. The interface between nsp10 and nsp16 was targeted and several interactions were observed. Biflavonoid robustaflavone (**4**) had the highest affinity (Fig. 4B). Its pyrone ring C' was in carbon-hydrogen bonding with Ile4334. Chromanone (ring A') hydroxyl formed a strong H-bonding with Asp4335 (3.50 Å). Carbon atoms of chromanone (rings A and C) and hydroxyphenyl ring B' formed salt bridges with Lys4346 while ring C' carbonyl exhibited a salt bridge with Arg4331.

Endoribonuclease (nsp15)

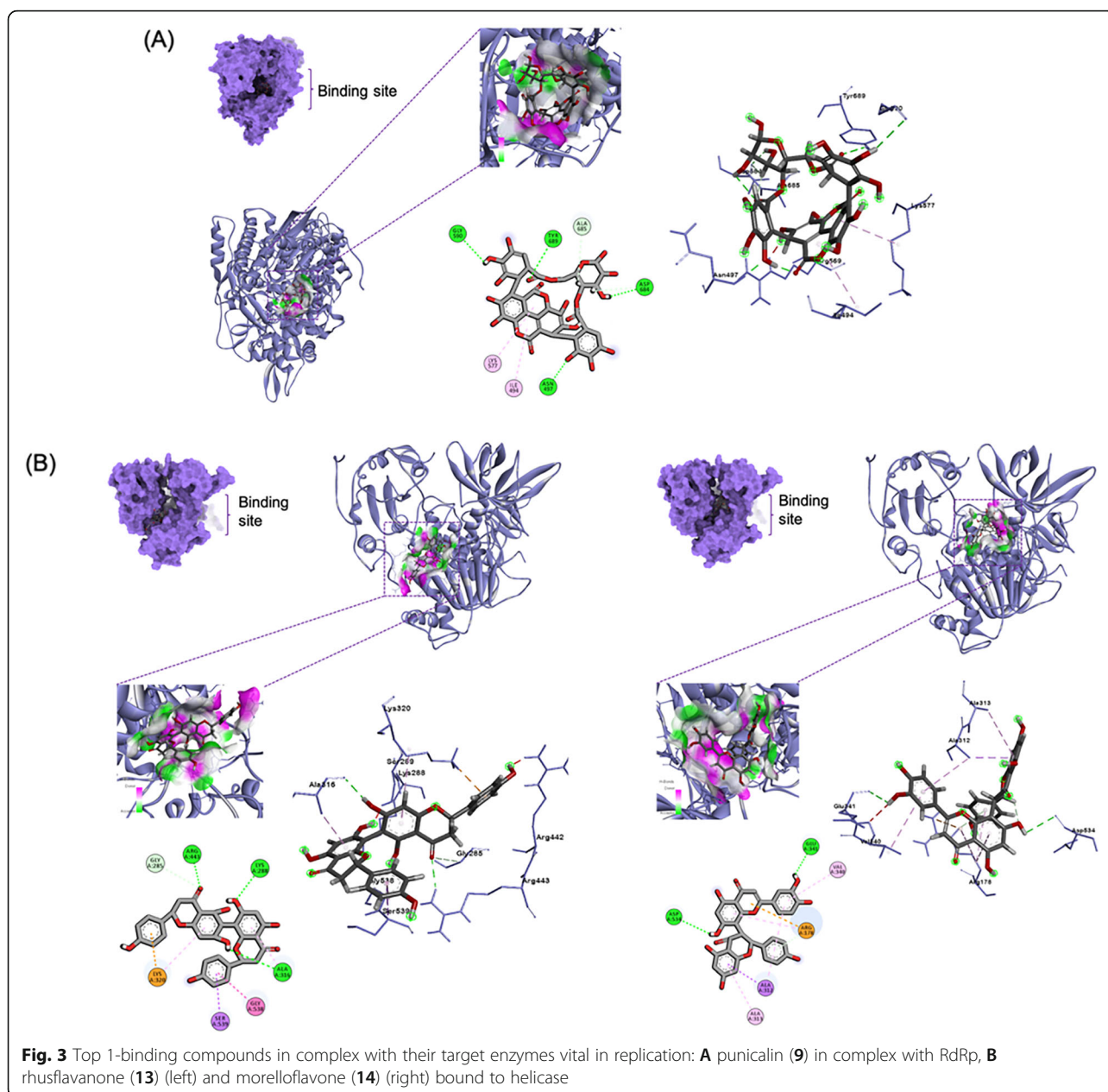
Top-scoring compounds against nsp15 exhibited affinities of -8.6 to -7.3 kcal/mol, stronger (Table 4). The

biflavonone hinokiflavone (**15**) scored the highest affinity, noting its interactions with its putative binding site that is proximal to the catalytic triad of His235, His250, and Lys290: flavone moiety (rings A, B, and C) in hydrogen bonding (4.55 Å) and *pi*-alkyl interaction with Met243, pyrone ring C in *pi*-sigma interaction with Tyr262, pyrone ring C' in *pi*-anion interaction with Glu258, and hydroxyphenyl ring B' in *pi*-alkyl and *pi*-*pi* stacked interactions with Ala256 and His362, respectively (Fig. 4C).

Druggability, ADME, and toxicity

Six of the 20 top-scoring and multi-targeting repurposed phytochemicals were found to be druggable according to Lipinski's rule of five (Table 5). Hinokiflavone (**15**) is a top-scoring, multi-targeting, druggable compound. Moreover, compounds **5** and **17** were multi-targeting and exhibited good gastrointestinal absorption properties.

In addition, compounds **25** and **26** showed the best solubility in water of -2.85, thereby depicting good excretion properties (Table 6). Toxicity prediction through OSIRIS Property Explorer showed that all top



compounds except **11**, **14**, **15**, **18**, **19**, and **20** have no mutagenic, tumorigenic, irritant, and reproductive toxicity risks (Table 6).

Molecular dynamics simulations

Molecular dynamics (MD) simulation was performed on the top-binding ligands, chosen based on molecular docking and ADMET analyses, to assess at an atomic level the binding behavior of the various polyphenols against SARS-CoV-2 non-structural proteins. The stability of the complexes, specifically PLpro-amentoflavone (**1**), 3CLpro-amentoflavone (**1**), RdRp-punicalin (**9**), helicase-rhusflavanone (**13**), nsp16-michellamine B (**19**),

nsp10-robustafavone (**4**), and nsp15-hinokiflavone (**15**), was evaluated using post-simulation parameters root mean square deviation (RMSD) and root mean square fluctuations (RMSF). RMSD is one of the widely used analyses using MD trajectories of protein-ligand complexes to establish equilibrium within a given simulation period. Based on RMSD analysis which was measured as an average throughout a 20-ns simulation, the complexes attained dynamic stability (Fig. 5). In the case of the amentoflavone (**1**)-bound PLpro, it took some time for the complex to reach equilibrium. As shown in the plot of RMSD (Å) versus simulation time (ns), a steady increase in RMSD can be observed up to 15 ns before

Table 3 Binding affinities and interactions of top ten ligands against the nsps of the SAM-dependent 2'-O-methyltransferase complex

Target	Cpd	Binding affinity (kcal/mol)	Hydrogen bonds	Other interactions
nsp16	19	-10.6	Asp6897, Asp6928	Cys6913, Cys6914, Met6929, Asp6931, Phe6947, Gly6869, Leu6898
	4	-10.6	Lys6844, Cys6913, Asp6928, Asp6928, Asn6996	Asn6841, Asp6897, Gly6869, Met6929, Leu6898, Glu7001
	1	-10.2	Asn6841, Asp6897, Leu6898, Asp6912	Pro6932, Asp6897, Leu6898, Met6929, Phe6947
	23	-10.2	Asp6931, Cys6913, Tyr6930	Asp6931, Phe6947, Asp6912, Leu6898, Met6929, Asp6897, Gly6869, Asp6928
	25	-9.5	Gly6911, Asp6873, Gly6871, Tyr6930	Leu6898, Cys6913, Met6929, Tyr6930,
	3	-9.5	Asn6841, Lys6844, Asn6996	Met6839, Met6840, Tyr6930, Pro6932, Ser6999
	18	-9.5	Asn6841, Asp6897, Asn6899, Tyr6930, Asn6996, Ser6999, Glu7001	Lys6844, Lys6968
	13	-9.5	Ser759, Asp761	Leu758, Ala688, Asp760, Cys813
	26	-9.4	Asn6899, Asp6873, Lys6844, Asn6841, Asp6928, Leu6898, Asp6912	Cys6913, Phe6947, Gly6869, Tyr6930, Asp6897,
	20	-9.3	Lys6844, Gly6869, Asp6873	Lys6935
nsp10	4	-7.7	Asp4335	Arg4331, Ile4334, Lys4346
	1	-7.4	His4333, Ile4334	Arg4331
	27	-7.3	Asp4344, Leu4345	Tyr4329, Cys4327, His4336, Pro4337, Leu4345, Leu4365
	15	-7.3	Arg4331, His4333, Lys4348, Gly4323, Tyr4349	Val4295, Gly4322, Ala4324
	19	-7.2	Lys4346	Cys4330, His4333, Ala4324, Lys4346, Val4295
	11	-7.2	Asn4293	Cys4294, Lys4296, Val4295, Leu4298
	23	-7.1	Cys4330, His4333, Ile4334, Asp4335, His4336	Lys4346
	25	-7	Tyr4329, His4333, Ala4324, Leu4345, Lys4348	Lys4346, Tyr4349
	8	-7	Cys4343	Lys4346, Gly4347, Phe4342
	26	-6.9	Leu4345, Lys4348, Gly4347, Ala4324, His4333, Ile4334, Tyr4329	Lys4348, Arg4331, Lys4346,
17	-6.9	Tyr4329, His4336	Asn4293, Arg4331, Ala4324, His4333, Lys4346, Ile4334	
9	-6.9	Ala4324, Lys4346, Lys4348, Tyr4349	Val4295, Gly4322, Gly4347, Ala4324, Tyr4349	
20	-6.9	Leu4345, Gly4347, Lys4348	Ala4324, Arg4331, His4333	

stabilization occurs. A similar trend can be observed for the RdRp-punicalin (**9**) complex. After a steady rise in RMSD, the complex achieved equilibrium around 13 ns with an average RMSD value of 7.1 Å. Among the complexes, the amentoflavone (**1**)-bound 3CLpro appeared to be the most stable complex having the lowest average equilibrium RMSD (2.2 Å). Although a minor fluctuation can be observed around 11 ns, the complex remained stable for the entire simulation time. In the case of nsp16-michellamine B (**19**) complex, an incremental increase in RMSD can be noted from the start of the simulation until 8 ns and a relatively high divergence can be seen around 9 ns. However, the system gained equilibrium thereafter. For the helicase-rhusflavanone (**13**) complex, several minor fluctuations can be noticed from initial binding stage up to mid simulation time. Despite this observation, the average RMSD of the complex remained low (2.8 Å). Another relatively stable

complex is robustaflavone (**4**) bound to nsp10 with an average equilibrium RMSD of 3.9 Å. Shortly after ligand-binding, the complex attained equilibrium. Lastly, the nsp15-hinokiflavone (**15**) complex exhibited relatively low stability based on the RMSD plot where some minor fluctuations are noted at the beginning of the simulation up to 15 ns.

The time-averaged residual fluctuations of the seven top-binding complexes were also analyzed on the basis of trajectory data within a 20-ns simulation (Fig. 6). The results of the residual RMSF analysis revealed that most of the complexes, particularly 3CLpro-amentoflavone (**1**), nsp16-michellamine B (**19**), nsp10-robustaflavone (**4**), helicase-rhusflavanone (**13**), have average RMSF values ranging from 1.1 to 1.6 Å and have shown relatively stable fluctuation patterns. These data are consistent with RMSD analysis, which confirm that the said complexes are stable. For the hinokiflavone (**15**)-bound

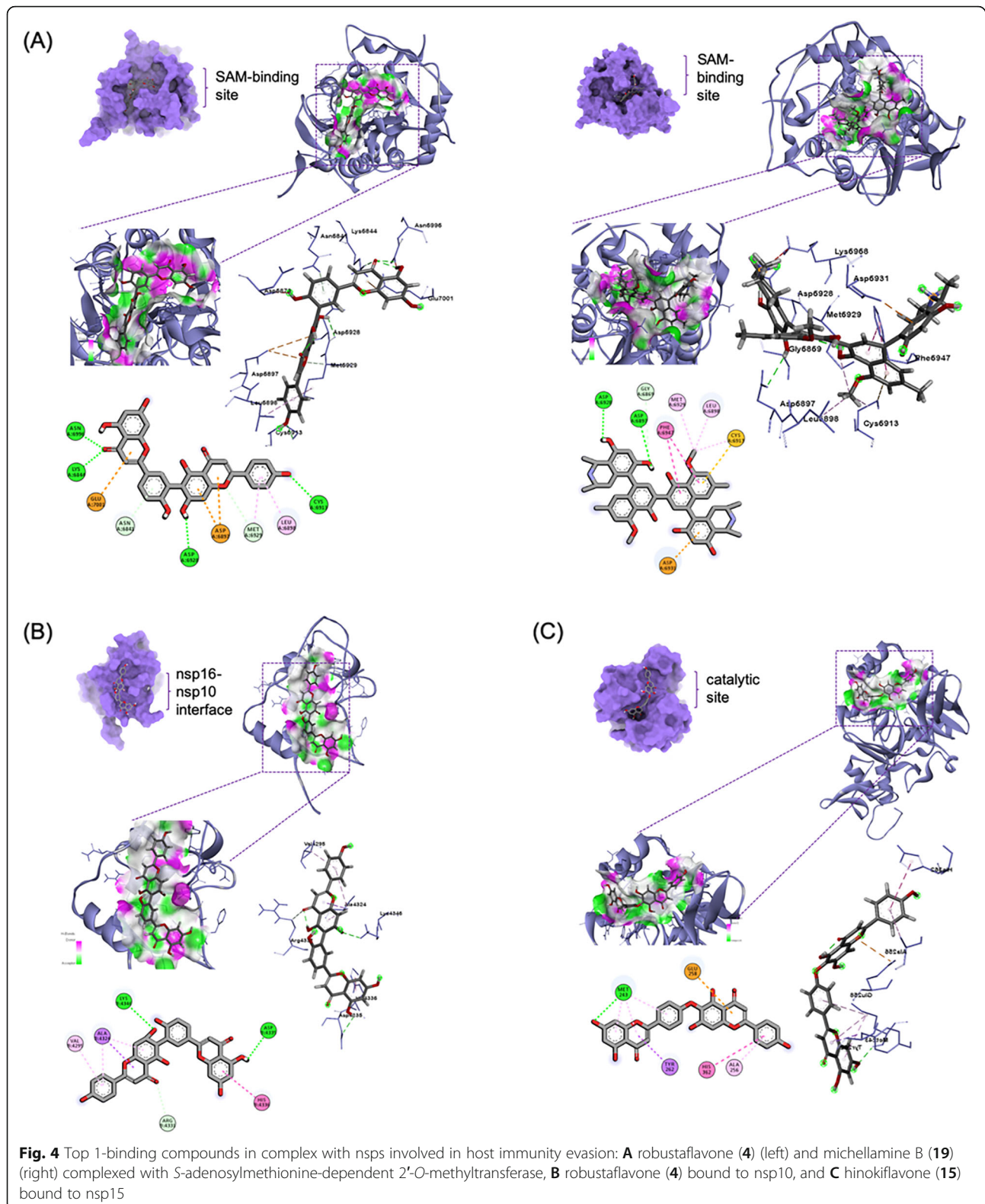


Table 4 Binding affinities and interactions of top ten ligands against nsp15

Target	Cpd	Binding affinity (kcal/mol)	Hydrogen bonds	Other interactions
nsp15	15	-8.6	Met243	Met243, Tyr262, Glu258, His362, Ala256
	4	-8.5	None	Lys281, Glu285, Tyr262, Met243
	1	-8.4	Gly254	Met243, Ala256, Glu258
	25	-8.1	Phe265, Ser266	Lys281, Ser266, Ala256
	23	-8	None	Glu258, Ala256, Gly263, Asp264, Phe265
	26	-7.8	Glu285, Glu364	Ala256, Ser266, Met243, Lys281, Glu285
	12	-7.7	Glu285	Ala256, Met243, Tyr262, Lys281
	14	-7.7	Arg282	Glu285, Lys281, Phe265
	13	-7.3	Gly263, Asp264	Ala256, His259, Asp264, Met243, Glu285
	17	-7.3	Glu258	None

nsp15 complex, the average residual fluctuations are slightly higher (2.2 Å). For the larger protein complexes—RdRp and PLpro, higher fluctuations were observed, averaging 3.3 Å and 3.5 Å, respectively. Such an RMSF pattern for the two complexes justifies the observed longer time for stabilization to occur during RSMD calculations.

Discussion

The SARS-CoV-2 non-structural proteins (nsps) play vital roles in the virus' pathogenesis, survival, and virulence. A number of these nsps have been considered as attractive and important drug targets due to their involvement in viral post-translational processing, replication, and host immunity evasion mechanisms (Fig. 7).

Table 5 Druggability of top, multi-targeting compounds according to Lipinski's rule of five

Cpd	MW < 500	#H-bond acceptors <10	#H-bond donors <5	Lipophilicity MLogP<5	Lipinski violations	Drug-likeness	Target
1	538.46	10	6	0.25	2	No	PLpro, 3CLpro, RdRp, helicase, nsp10, nsp16, nsp15
2	426.72	1	0	6.92	1	Yes	PLpro, RdRp
3	570.8	4	0	5.03	2	No	PLpro, 3CLpro, RdRp, nsp16
4	538.46	10	6	0.25	2	No	PLpro, 3CLpro, RdRp, helicase, nsp10, nsp16, nsp15
5	472.7	4	3	4.97	1	Yes	PLpro, RdRp
8	538.46	10	6	0.25	2	No	PLpro, 3CLpro, helicase, nsp10
9	782.53	22	13	-2.56	3	No	PLpro, RdRp, nsp10
10	456.7	3	2	5.82	1	Yes	PLpro, RdRp
11	540.47	10	3	0.41	2	No	3CLpro, nsp10
12	498.74	4	1	5.97	1	Yes	3CLpro, nsp15
13	542.49	10	6	0.58	2	No	3CLpro, helicase, nsp16, nsp15
14	556.47	11	7	-0.08	3	No	3CLpro, helicase, nsp15
15	538.46	10	5	0.52	1	Yes	3CLpro, RdRp, helicase, nsp10, nsp15
17	520.65	8	4	1.95	1	Yes	3CLpro, nsp10, nsp15
18	992.64	28	14	-3.39	3	No	RdRp, np16
19	756.88	10	8	3.18	2	No	RdRp, helicase, nsp10, nsp16
20	1008.75	28	14	-3.39	3	No	RdRp, nsp10, nsp16
23	578.52	14	8	-2.96	3	No	helicase, nsp10, nsp16, nsp15
25	516.45	12	7	-0.35	3	No	nsp10, nsp16, nsp15
26	516.45	12	7	-0.35	3	No	nsp10, nsp16, nsp15

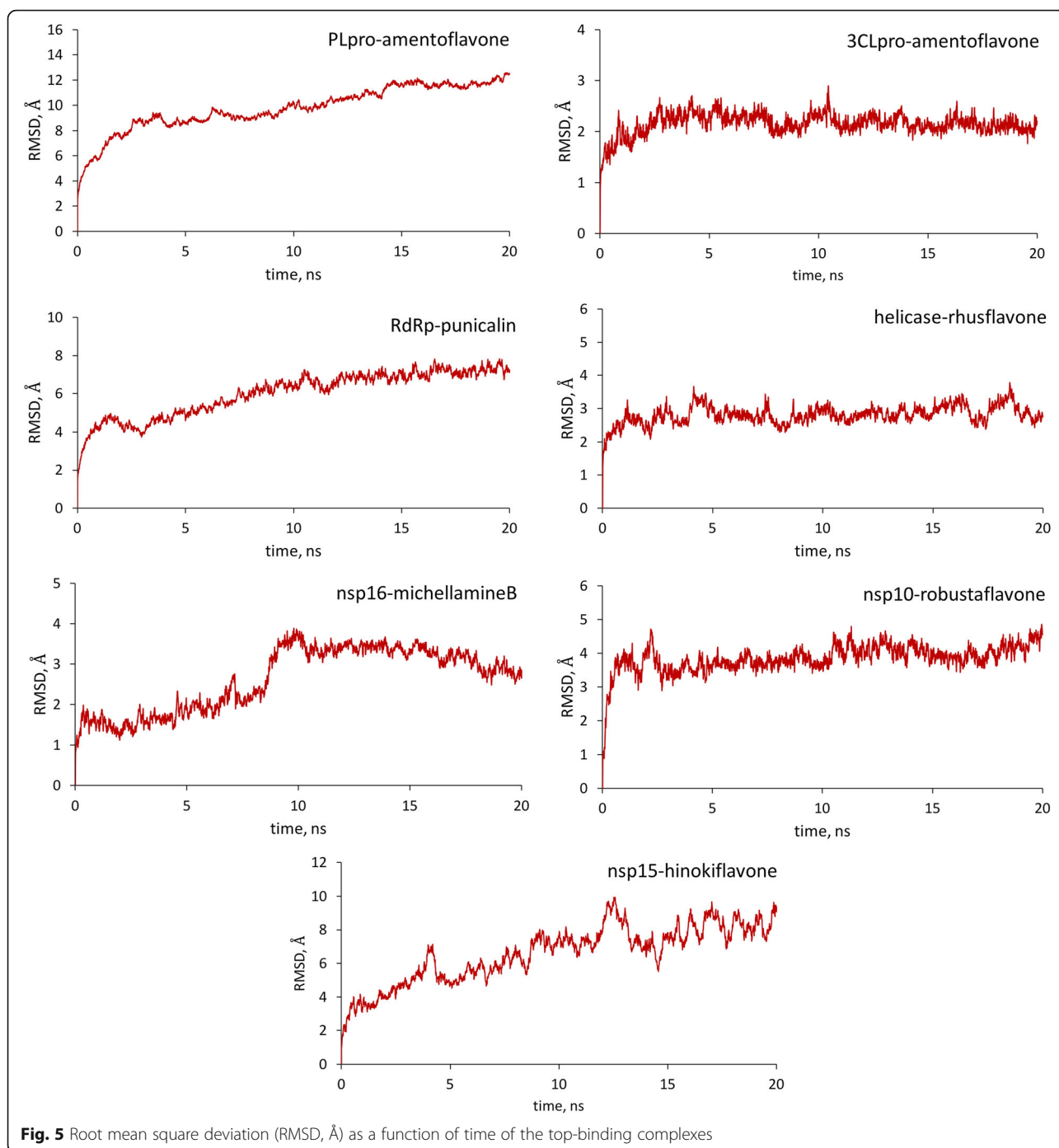
Table 6 Toxicity risks of top, multi-targeting compounds as predicted by OSIRIS Property Explorer

Cpd	Toxicity risk				Solubility (LogS)
	Mutagenic	Tumorigenic	Irritant	Reproductive effective	
1	No	No	No	No	-6.16
2	No	No	No	No	-6.97
3	No	No	No	No	-7.66
4	No	No	No	No	-6.18
5	No	No	No	No	-5.66
8	No	No	No	No	-6.18
9	No	No	No	No	-5.89
10	No	No	No	No	-6.11
11	No	No	No	High Risk	-5.11
12	No	No	No	No	-6.37
13	No	No	No	No	-5.75
14	No	No	No	High Risk	-4.82
15	No	No	No	High Risk	-6.69
17	No	No	No	No	-4.42
18	No	No	High Risk	No	-3.54
19	No	High Risk	No	No	-11.38
20	No	No	High Risk	No	-3.54
23	No	No	No	No	-2.95
25	No	No	No	No	-2.85
26	No	No	No	No	-2.85

The cysteine proteases, nsp3 (PLpro) and nsp5 (3CLpro), are involved in the autolytic cleavage of the polyproteins pp1a and pp1ab wherein PLpro cleaves 3 sites at the *N*-terminus while 3CLpro cleaves through the remaining sites (11 sites in pp1ab) to release the nsps [36]. Proceeding to the replication-transcription complex, nsp12 (RdRp) elongates the daughter strand through the polymerization of nucleotides while nsp13 (helicase) clears RNA secondary structures and RNA-binding proteins [37]. The nsp 16 (SAM-dependent 2'-*O*-methyltransferase) in complex with nsp10 as its cofactor provides a 5' cap to the RNA genome through C2'-*O*-methyl-ribosyladenine, conferring RNA stability and host cell immunity protection [38]. Lastly, the nsp15 (endoribonuclease) hinders recognition of dsRNA intermediates by host dsRNA sensors [33]. Our results, therefore, highlight the role of anti-HIV RT phytochemicals as potential antagonists of SARS-CoV-2 by interfering with the discussed mechanisms.

Natural products have been a subject of investigation concerning their ability to antagonize SARS-CoV-2 due to their availability and wide range of health benefits [34, 35, 39–41]. In relation, repurposing established anti-HIV phytochemicals means that the lead compounds in this study can be easily obtained from previously explored plants that are consumed by populations. Here, we

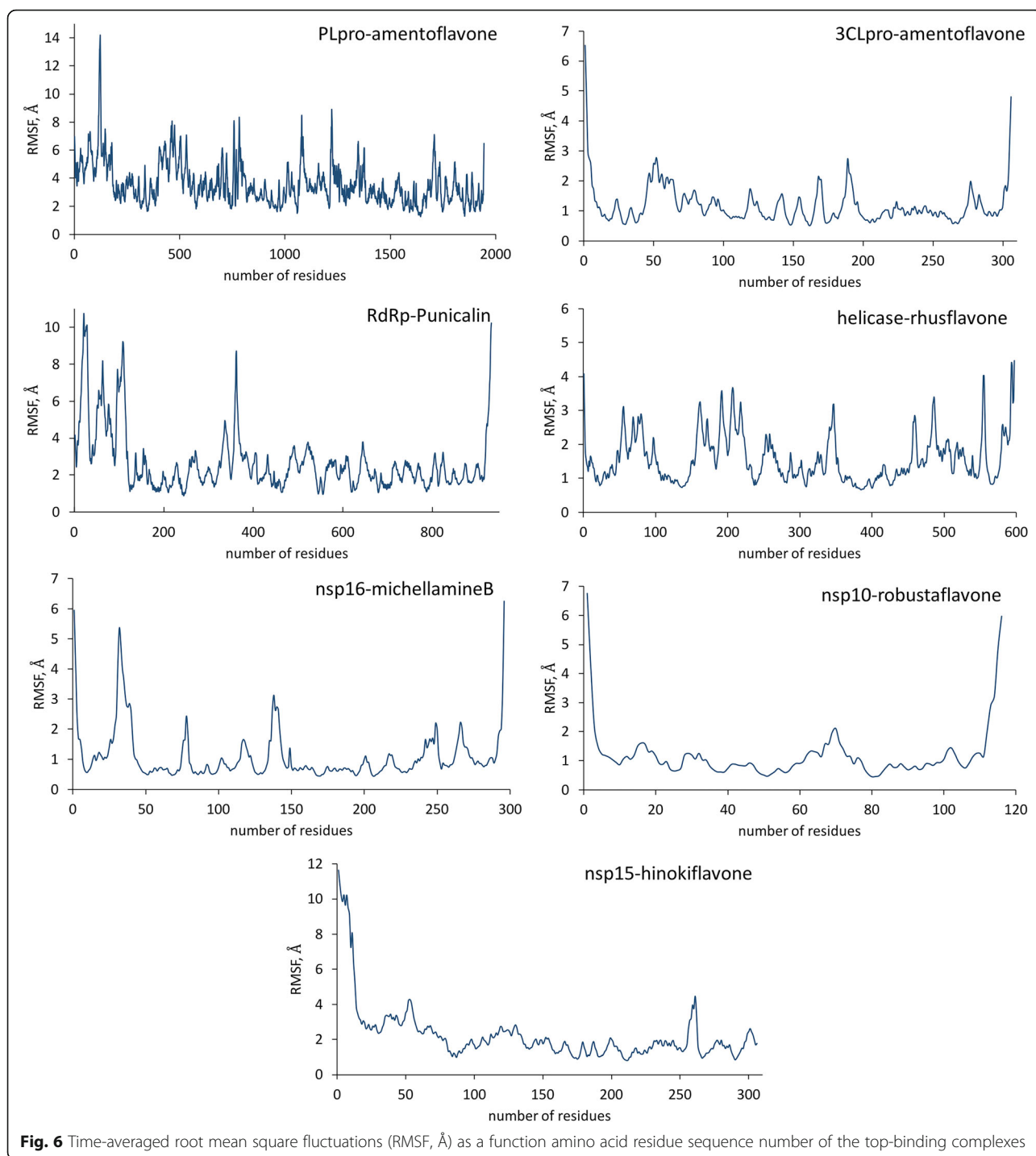
focused on the employment of computational target-based drug discovery methodologies, such as molecular docking, molecular dynamic simulations, and pharmacokinetic property predictions in search for potential hits for inhibiting the aforementioned SARS-CoV-2 nsps. Our study revealed that the biflavonoid amentoflavone (1) showed the highest binding to both SARS-CoV-2 cysteine proteases PLpro and 3CLpro. Compound 1, isolated from the Chinese olive fruit, *Canarium album* [42], was also reported in a previous study to be a potent inhibitor of SARS-CoV PLpro [43, 44]. Volkensiflavone (11) from the seeds and rinds of *Garcinia intermedia* [45] was another top compound against 3CLpro. Punicalin (9) from the pomegranate *Punica granatum* peel [46] exhibited high binding propensity against RdRp, an enzyme considered to be a promising target inhibiting viral replication. Morelloflavone (14) from *G. intermedia* was first to be reported here with an inhibitory potential against SARS-CoV-2 helicase. Interestingly, its potential extends against 3CLpro [47]. Robustaflavone (4) from the leaves of *Garcinia epunctata* [48] showed the best potential against the 2'-*O*-methyltransferase and its cofactor. This is the first investigation of its activity against these nsps aside from its interaction with 3CLpro [49]. On the other hand, michellamine B (19) from *Ancistrocladus korupensis* leaves [50] manifested an inhibitory



potential against nsp16, therefore opening the doors of phenolic alkaloids against SARS-CoV-2. Lastly, hinokiflavone (15) from *Selaginella tamariscina* [51] was reported to be a potential 3CLpro inhibitor and potent against the replication-transcription complex [43, 47, 49, 52]. This, however, is the first investigation of its activity against the endoribonuclease of SARS-CoV-2 in silico. The multi-targeting potential of some of these

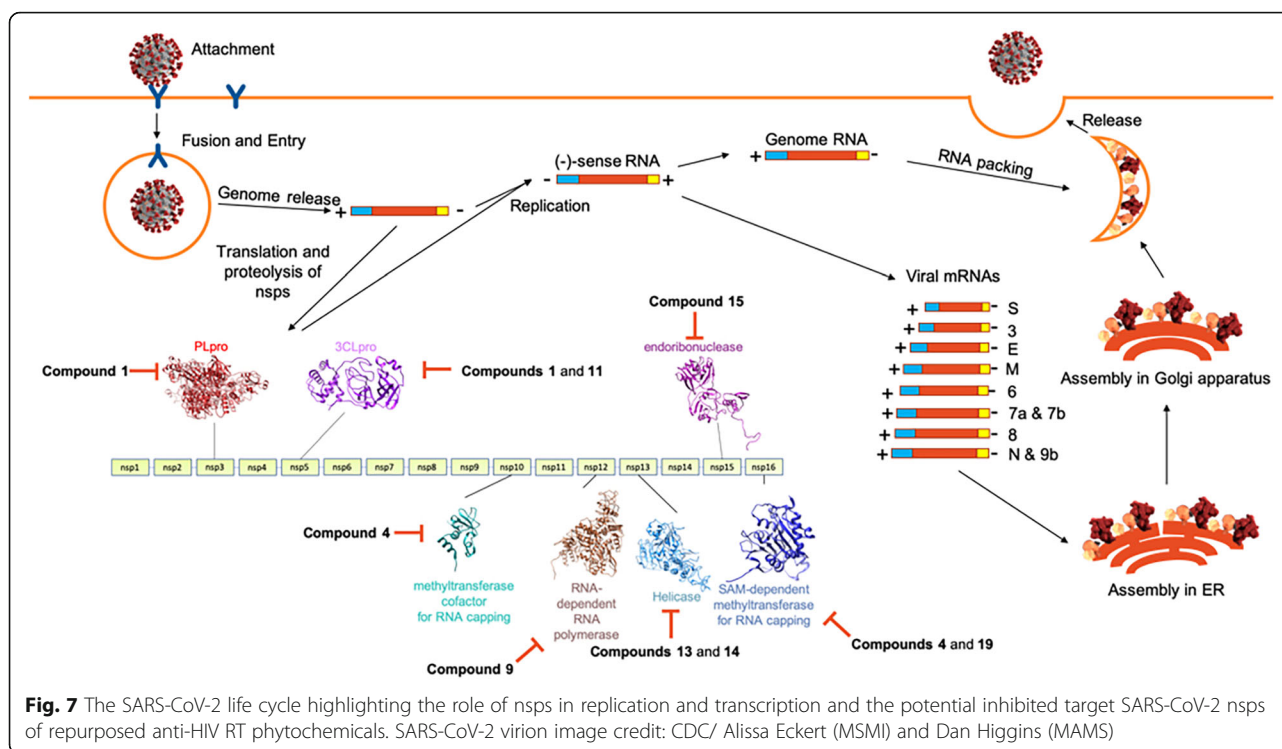
compounds increases the chance of getting a maximal inhibitory effect [53].

To further validate the molecular docking analysis, the top-binding ligands were submitted for molecular dynamic simulations. Through post-simulation analyses, the top-binding ligands were generally found to be dynamically stable upon binding to respective proteins. Although most of the top 1 compounds were predicted in



silico to be non-druggable, efforts are rising to explore compounds in the oral druggable space beyond the rule of five (bRo5) [54, 55]. Additionally, four of these did not manifest toxicity in silico. The biflavonoids volkensiflavone (11), morelloflavone (14), and hinokiflavone (15) were computationally predicted as non-mutagenic, non-tumorigenic, and non-irritant, but were predicted to pose reproductive toxicity risk which may be attributed

to their chromene and hydroxyphenyl moieties. It should be noted, however, that hinokiflavone (15) is a druggable top 1 compound. Michellamine B (19) was predicted to be tumorigenic due to its naphthalene moiety. In addition, compounds 5 and 17 exhibited good gastrointestinal absorptive features as implicated by their favorable lipophilicity and polar surface area [56]. These also did not manifest any form of toxicity in silico.



Despite computational incompatibilities, these compounds can still serve as templates for drug design and undergo *in vitro* and *in vivo* assays for validating their anti-SARS-CoV-2 properties, noting that their promising polyphenolic nature allowed them to form hydrogen bonds with key residues of the SARS-CoV-2 nsps. With the validation of pre-clinical experiments, the secondary metabolites can be produced through *in vitro* plant tissue cultures that can be augmented by metabolic engineering, elicitation, and even the use of bioreactors [57, 58].

Conclusions

The search for anti-COVID-19 therapeutic agents is a response to the continuous spread of the virus amidst vaccine availability. The similarity between the pathogenesis of HIV and SARS-CoV-2 inspired the repurposing of previously reported anti-HIV reverse transcriptase phytochemicals against SARS-CoV-2 nsps implicated in viral replication, post-translational processing, and host immunity evasion mechanisms. The top-ranking polyphenolics amentoflavone (1), robustaflavone (4), punicalin (9), volkensiflavone (11), rhusflavanone (13), morelloflavone (14), hinokiflavone (15), and michellamine B (19) can be further screened using confirmatory *in vitro* and *in vivo* assays, and can serve as prototypes for designing novel anti-COVID-19 drugs in consideration of their polyphenolic nature. As promising drug templates, functionalities in the compound structure can be modified to improve druggability and pharmacokinetic properties.

Abbreviations

3CLpro: 3-Chymotrypsin-like protease; ADME: Absorption, digestion, metabolism, and excretion; BE: Binding energy; COVID-19: Coronavirus disease 2019; Cpd: Compound; dsDNA: Double-stranded DNA; HIV: Human immunodeficiency virus; kcal/mol: Kilocalorie per mole; nsp: Non-structural protein; PDB: Protein data bank; PLpro: Papain-like protease; RdRp: RNA-dependent RNA polymerase; RNA: Ribonucleic acid; RT: Reverse transcriptase; SARS-CoV-2: Severe acute respiratory syndrome coronavirus 2

Additional files

Additional file 1

Acknowledgements

Not applicable.

Authors' contributions

VNODL, JAHM, DYHP: conceptualization, investigation, data collection and analysis, manuscript preparation, and manuscript editing. RATF: conceptualization, investigation, data collection and analysis, manuscript preparation, and manuscript editing and review. JKARC: data collection. MTJQ: conceptualization, investigation, data collection and analysis, manuscript editing, and manuscript review. JCMA: investigation and manuscript editing. KIRN: conceptualization, investigation, manuscript editing and manuscript review. APMG: conceptualization, design, manuscript preparation, editing, and review. All authors have read and approved the present version of the manuscript.

Funding

Not applicable.

Availability of data and materials

All data generated in this study are included in this published article and the supplementary information files.

Declarations

Ethics approval and consent to participate

Not applicable.

Consent for publication

Not applicable.

Competing interests

Not applicable.

Author details

¹Laboratory for Organic Reactivity, Discovery and Synthesis (LORDS), Research Center for the Natural and Applied Sciences, University of Santo Tomas, España Blvd., 1015 Manila, Philippines. ²Department of Biological Sciences, College of Science, University of Santo Tomas, España Blvd., 1015 Manila, Philippines. ³Department of Chemistry, College of Science, University of Santo Tomas, España Blvd., 1015 Manila, Philippines. ⁴The Graduate School, University of Santo Tomas, España Blvd., 1015 Manila, Philippines. ⁵Chemistry Department, College of Science and Mathematics, Mindanao State University – Iligan Institute of Technology, Tibanga, 9200 Iligan City, Philippines. ⁶Philippine Science High School – Central Mindanao Campus, 9217 Balo-I, Lanao del Norte, Philippines. ⁷Faculty of Medicine and Surgery, University of Santo Tomas, España Blvd., 1015 Manila, Philippines.

Received: 2 March 2021 Accepted: 6 July 2021

Published online: 16 July 2021

References

- Guo Q, Xu W, Wang P-F, Ji H-Y, Zhang X-L, Wang K, Li J (2021) Facing coronavirus disease 2019: What do we know so far? (Review). *Exp Ther Med* 21(6):658–663. <https://doi.org/10.3892/etm.2021.10090>
- Wang C, Xiao X, Feng H, Hong Z, Li M, Tu N, Li X, Wang K, Bu L (2021) Ongoing COVID-19 pandemic: a concise but updated comprehensive review. *Curr Microbiol* 78(5):1718–1729. <https://doi.org/10.1007/s00284-021-02413-z>
- World Health Organization. WHO coronavirus disease (COVID-19) dashboard. <https://covid19.who.int/>. Accessed 26 May 2021.
- Astuti I, Ysrafil (2020) Severe acute respiratory syndrome coronavirus 2 (SARS-CoV-2): An overview of viral structure and host response. *Diabetes Metab Syndr* 14:407–412. <https://doi.org/10.1016/j.dsx.2020.04.020>
- Shahzad F, Anderson D, Najafzadeh M (2020) The antiviral, anti-inflammatory effects of natural medicinal herbs and mushrooms and SARS-CoV-2 infection. *Nutrients* 12(9). <https://doi.org/10.3390/nu12092573>
- Pandey A, Khan MK, Hamurcu M, Gezgin S (2020) Natural plant products: a less focused aspect for the COVID-19 viral outbreak. *Front Plant Sci* 11. <https://doi.org/10.3389/fpls.2020.568890>
- Forrestall K, Burley D, Cash M, Pottie I, Darvesh S (2020) 2-Pyridone natural products as inhibitors of SARS-CoV-2 main protease. *Chem Biol Interact* 335: 109348. <https://doi.org/10.1016/j.cbi.2020.109348>
- Notarte KI, Devanadera MK, Mayor AB, Cada MC, Pecundo MH, Macabeo AP (2019) Toxicity, antibacterial, and antioxidant activities of fungal endophytes *Colletotrichum* and *Nigrospora* spp. isolated from *Uvaria grandiflora*. *Philipp J Sci* 148:503–510
- Quimque MT, Notarte KI, Letada A, Fernandez RA, Pilapil DY, Pueblos KR et al. (2021) Potential cancer- and Alzheimer's disease-targeting phosphodiesterase inhibitors from *Uvaria alba*: Insights from *in vitro* and consensus virtual screening. *ACS Omega* 6(12):8403–8417. <https://doi.org/10.1021/acsomega.1c00137>
- Paraiso IL, Revel JS, Stevens JF (2020) Potential use of polyphenols in the battle against COVID-19. *Curr Opin Food Sci* 32:149–155. <https://doi.org/10.1016/j.cofs.2020.08.004>
- Levy E, Delvin E, Marciel V, Spahis S (2020) Can phytotherapy with polyphenols serve as a powerful approach for the prevention and therapy tool of novel coronavirus disease 2019 (COVID-19)? *Am J Physiol Endocrinol Metab* 319(4):E689–E708. <https://doi.org/10.1152/ajpendo.00298.2020>
- Annunziata G, Sanduzzi Zamparelli M, Santoro C, Ciampaglia R, Stornaiuolo M, Tenore GC, Sanduzzi A, Novellino E (2020) May polyphenols have a role against coronavirus infection? An overview of *in vitro* evidence. *Front Med (Lausanne)* 7. <https://doi.org/10.3389/fmed.2020.00240>
- Mehany T, Khalifa I, Barakat H, Althwab SA, Alharbi YM, El-Sohaimy S (2021) Polyphenols as promising biologically active substances for preventing SARS-CoV-2: a review with research evidence and underlying mechanisms. *Food Biosci* 40:100891. <https://doi.org/10.1016/j.fbio.2021.100891>
- Benarba B, Pandiella A (2020) Medicinal plants as sources of active molecules against COVID-19. *Front Pharmacol* 11. <https://doi.org/10.3389/fphar.2020.01189>
- Boukhatem MN, Setzer WN (2020) Aromatic herbs, medicinal plant-derived essential oils, and phytochemical extracts as potential therapies for coronaviruses: Future perspectives. *Plants (Basel)* 9. <https://doi.org/10.3390/plants9060800>
- Quimque MTJ, Notarte KIR, Fernandez RAT, Mendoza MAO, Liman RAD, Lim JAK, Pilapil LAE, Ong JKH, Pastrana AM, Khan A, Wei DQ, Macabeo APG (2020) Virtual screening-driven drug discovery of SARS-CoV2 enzyme inhibitors targeting viral attachment, replication, post-translational modification and host immunity evasion infection mechanisms. *J Biomol Struct Dyn* 16:1–18. <https://doi.org/10.1080/07391102.2020.1776639>
- Gogoi M, Borkotoky M, Borchetia S, Chowdhury P, Mahanta S, Barooah AK (2021) Black tea bioactives as inhibitors of multiple targets of SARS-CoV-2 (3CLpro, PLpro and RdRp): a virtual screening and molecular dynamic simulation study. *J Biomol Struct Dyn* 10:1–24. <https://doi.org/10.1080/07391102.2021.1897679>
- Stasiulewicz A, Maksymiuk AW, Nguyen ML, Belza B, Sulkowska JI (2021) SARS-CoV-2 papain-like protease potential inhibitors-*In silico* quantitative assessment. *Int J Mol Sci* 22(8):3957–3986. <https://doi.org/10.3390/ijms22083957>
- Ghazwani MY, Bakheit AH, Hakami AR, Alkahtani HM, Almezhia AA (2021) Virtual screening and molecular docking studies for discovery of potential RNA-dependent RNA polymerase inhibitors. *Crystals* 11(5):471. <https://doi.org/10.3390/cryst11050471>
- Pettersen EF, Goddard TD, Huang CC, Couch GS, Greenblatt DM, Meng EC, Ferrin TE (2004) UCSF Chimera-A visualization system for exploratory research and analysis. *J Comput Chem* 25(13):1605–1612. <https://doi.org/10.1002/jcc.20084>
- Yoshimoto FK (2020) The proteins of severe acute respiratory syndrome coronavirus-2 (SARS CoV-2 or n-COV19), the cause of COVID-19. *Protein J* 39(3):198–216. <https://doi.org/10.1007/s10930-020-09901-4>
- Gorbalenya AE, Koonin EV, Donchenko AP, Blinov VM (1989) Coronavirus genome: prediction of putative functional domains in the non-structural polyprotein by comparative amino acid sequence analysis. *Nucleic Acids Res* 17(12):4847–4861. <https://doi.org/10.1093/nar/17.12.4847>
- Seybert A, Hegyi A, Siddell SG, Ziebuhr J (2000) The human coronavirus 229E superfamily 1 helicase has RNA and DNA duplex-unwinding activities with 5'-to-3' polarity. *RNA* 6(7):1056–1068. <https://doi.org/10.1017/s1355838200000728>
- van Dinten LC, van Tol H, Gorbalenya AE, Snijder EJ (2000) The predicted metal-binding region of the arterivirus helicase protein is involved in subgenomic mRNA synthesis, genome replication, and virion biogenesis. *J Virol* 74(11):5213–5223. <https://doi.org/10.1128/jvi.74.11.5213-5223.2000>
- Chinsembu KC (2019) Chemical diversity and activity profiles of HIV-1 reverse transcriptase inhibitors from plants. *Rev Bras Farmacogn* 29(4):504–528. <https://doi.org/10.1016/j.bjpp.2018.10.006>
- Hanwell MD, Curtis DE, Lonie DC, Vandermeersch T, Zurek E, Hutchison GR (2012) Avogadro: an advanced semantic chemical editor, visualization, and analysis platform. *J Cheminformatics* 4. <https://doi.org/10.1186/1758-2946-4-17>
- Wang J, Wang W, Kollman PA, Case DA (2006) Automatic atom type and bond type perception in molecular mechanical calculations. *J Mol Graph Model* 25(2):247–260. <https://doi.org/10.1016/j.jmgm.2005.12.005>
- Yang J, Roy A, Zhang Y (2013) Protein-ligand binding site recognition using complementary binding-specific substructure comparison and sequence profile alignment. *Bioinformatics* 29(20):2588–2595. <https://doi.org/10.1093/bioinformatics/btt447>
- Macabeo APG, Cruz AJC, Narmani A, Arzanlou M, Babai-Ahari A, Pilapil LAE, Garcia KYM, Huch V, Stadler M (2020) Tetrasubstituted α -pyrone derivatives from the endophytic fungus, *Neurospora udagawae*. *Phytochem Lett* 35: 147–151. <https://doi.org/10.1016/j.phytl.2019.11.010>
- Phukhamsakda C, Macabeo APG, Huch V, Cheng T, Hyde KD, Stadler M (2019) Sparicolins A-G, biologically active oxidized spirodioxynaphthalene derivatives from the ascomycete *Sparticola junci*. *J Nat Prod* 82(10):2878–2885. <https://doi.org/10.1021/acs.jnatprod.9b00604>

31. Van Der Spoel D, Lindahl E, Hess B, Groenhof G, Mark AE, Berendsen HJ (2005) GROMACS: Fast, flexible, and free. *J Comput Chem* 26(16):1701–1718. [https://doi.org/10.1002/\(ISSN\)1096-987X](https://doi.org/10.1002/(ISSN)1096-987X)
32. Toukmaji A, Sagui C, Board J, Darden T (2000) Efficient particlemesh ewald based approach to fixed and induced dipolar interactions. *J Chem Phys* 113(24):10913–10927. <https://doi.org/10.1063/1.1324708>
33. Deng X, Hackbart M, Mettelman RC, O'Brien A, Mielech AM, Yi G, Kao CC, Baker SC (2017) Coronavirus nonstructural protein 15 mediates evasion of dsRNA sensors and limits apoptosis in macrophages. *Proc Natl Acad Sci USA* 114(21):E4251–E4260. <https://doi.org/10.1073/pnas.1618310114>
34. Kim Y, Wower J, Maltseva N, Chang C, Jedrzejczak R, Wilamowski M, Kang S, Nicolaescu V, Randall G, Michalska K, Joachimiak A (2021) Tipiracil binds to uridine site and inhibits Nsp15 endoribonuclease NendoU from SARS-CoV-2. *Commun Biol* 4(1):193. <https://doi.org/10.1038/s42003-021-01735-9>
35. Antonio AS, Wiedemann LSM, Veiga-Junior VF (2020) Natural products' role against COVID-19. *RSC Adv* 10(39):23379–23393. <https://doi.org/10.1039/D0RA03774E>
36. Wu C, Liu Y, Yang Y, Zhang P, Zhong W, Wang Y, Wang Q, Xu Y, Li M, Li X, Zheng M, Chen L, Li H (2020) Analysis of therapeutic targets for SARS-CoV-2 and discovery of potential drugs by computational methods. *Acta Pharm Sin B* 10(5):766–788. <https://doi.org/10.1016/j.apsb.2020.02.008>
37. Chen J, Malone B, Llewellyn E, Grasso M, Shelton PMM, Olinares PDB, Maruthi K, Eng ET, Vatandaslar H, Chait BT, Kapoor TM, Darst SA, Campbell EA (2020) Structural basis for helicase-polymerase coupling in the SARS-CoV-2 replication-transcription complex. *Cell* 182(6):1560–1573. <https://doi.org/10.1016/j.cell.2020.07.033>
38. Rosas-Lemus M, Minasov G, Shuvalova L, Inniss NL, Kiryukhina O, Brunzelle J, Satchell KJF (2020) High-resolution structures of the SARS-CoV-2 2'-O-methyltransferase reveal strategies for structure-based inhibitor design. *Sci Signal* 13. 13(651):eabe1202. <https://doi.org/10.1126/scisignal.abe1202>
39. Boozari M, Hosseinzadeh H (2021) Natural products for COVID-19 prevention and treatment regarding to previous coronavirus infections and novel studies. *Phytother Res* 35(2):864–876. <https://doi.org/10.1002/ptr.6873>
40. Huang J, Tao G, Liu J, Cai J, Huang Z, Chen JX (2020) Current prevention of COVID-19: natural products and herbal medicine. *Front Pharmacol* 11. <https://doi.org/10.3389/fphar.2020.588508>
41. Menezes CJMDS, Campos VR (2021) Natural biflavonoids as potential therapeutic agents against microbial diseases. *Sci Total Environ* 769:145168. <https://doi.org/10.1016/j.scitotenv.2021.145168>
42. He Z, Xia W, Chen J (2008) Isolation and structure elucidation of phenolic compounds in Chinese olive (*Canarium album* L.) fruit. *Eur Food Res Technol* 226(5):1191–1196. <https://doi.org/10.1007/s00217-007-0653-5>
43. Eydoux C, Fattorini V, Shannon A, Le TT, Didier B, Canard B, Guillemot JC (2021) A fluorescence-based high throughput-screening assay for the SARS-CoV RNA synthesis complex. A fluorescence-based high throughput-screening assay for the SARS-CoV RNA synthesis complex. *J Virol Methods* 288:288. <https://doi.org/10.1016/j.jviromet.2020.114013>
44. Ryu YB, Jeong HJ, Kim JH, Kim YM, Park JY, Kim D, Nguyen TT, Park SJ, Chang JS, Park KH, Rho MC, Lee WS (2010) Biflavonoids from *Torreya nucifera* displaying SARS-CoV 3CL(pro) inhibition. *Bioorg Med Chem* 18(22):7940–7947. <https://doi.org/10.1016/j.bmc.2010.09.035>
45. Acuña UM, Figueroa M, Kavalier A, Jancovski N, Basile MJ, Kennelly EJ (2010) Benzophenones and biflavonoids from *Rheedia edulis*. *J Nat Prod* 73(11):1775–1779. <https://doi.org/10.1021/np100322d>
46. Singh B, Singh JP, Kaur A, Singh N (2018) Phenolic compounds as beneficial phytochemicals in pomegranate (*Punica granatum* L.) peel: a review. *Food Chem* 261:75–86. <https://doi.org/10.1016/j.foodchem.2018.04.039>
47. Teli DM, Shah MB, Chhabria MT (2021) *In silico* screening of natural compounds as potential inhibitors of SARS-CoV-2 main protease and spike RBD: Targets for COVID-19. *Front Mol Biosci* 7. <https://doi.org/10.3389/fmolb.2020.599079>
48. Emade Kwene C, Tih AE, Abderamane B, Ghogomu RT (2020) Two new phenolic glycosides from the leaves of *Garcinia epunctata* Stapf. *Z Naturforsch C J Biosci* 75(1–2):51–56. <https://doi.org/10.1515/znc-2018-0217>
49. Lokhande K, Nawani N, K Venkateswara S, Pawar S (2020) Biflavonoids from *Rhus succedanea* as probable natural inhibitors against SARS-CoV-2: a molecular docking and molecular dynamics approach [pre-print]. *J Biomol Struct Dyn* 1–13. <https://doi.org/10.1080/07391102.2020.1858165>
50. McMahon JB, Currens MJ, Gulakowski RJ, Buckheit RW, Jr Lackman-Smith C, Hallock YF et al (1995) Michellamine B, a novel plant alkaloid, inhibits human immunodeficiency virus-induced cell killing by at least two distinct mechanisms. *Antimicrob Agents Chemother* 39(2):484–488. <https://doi.org/10.1128/aac.39.2.484>
51. Zhang GG, Jing Y, Zhang HM, Ma EL, Guan J, Xue FN, Liu HX, Sun XY (2012) Isolation and cytotoxic activity of selaginellin derivatives and biflavonoids from *Selaginella tamariscina*. *Planta Med* 78(04):390–392. <https://doi.org/10.1055/s-0031-1298175>
52. Ngo ST, Pham NQA, Le LT, Pham D-H, Vu VV (2020) Computational determination of potential inhibitors of SARS-CoV-2 main protease. *J Chem Inf Model* 60(12):5771–5780. <https://doi.org/10.1021/acs.jcim.0c00491>
53. Senanayake SL (2020) Overcoming nonstructural protein 15-nidoviral uridylylate-specific endoribonuclease (nsp15/NendoU) activity of SARS-CoV-2. *Future Drug Discov* 2(3). <https://doi.org/10.4155/fdd-2020-0012>
54. Doak BC, Over B, Giordanetto F, Kihlberg J (2014) Oral druggable space beyond the rule of 5: insights from drugs and clinical candidates. *Chem Biol* 21(9):1115–1142. <https://doi.org/10.1016/j.chembiol.2014.08.013>
55. Tyagi M, Begnini F, Poongavanam V, Doak BC, Kihlberg J (2020) Drug syntheses beyond the rule of 5. *Chemistry* 26(1):49–88. <https://doi.org/10.1002/chem.201902716>
56. Daina A, Zoete V (2016) A BOILED-Egg to predict gastrointestinal absorption and brain penetration of small molecules. *ChemMedChem* 11(11):1117–1121. <https://doi.org/10.1002/cmdc.201600182>
57. Bhojwani SS, Dantu PK (eds) (2013) Plant tissue culture: an introductory text. Springer, India. <https://doi.org/10.1007/978-81-322-1026-9>
58. Pant B (2014) Application of plant cell and tissue culture for the production of phytochemicals in medicinal plants. In: Adhikari R, Thapa S (eds) Infectious diseases and nanomedicine II, Advances in experimental medicine and biology, vol 808. Springer, New Delhi, pp 25–39. https://doi.org/10.1007/978-81-322-1774-9_3

Publisher's Note

Springer Nature remains neutral with regard to jurisdictional claims in published maps and institutional affiliations.

Submit your manuscript to a SpringerOpen® journal and benefit from:

- Convenient online submission
- Rigorous peer review
- Open access: articles freely available online
- High visibility within the field
- Retaining the copyright to your article

Submit your next manuscript at ► [springeropen.com](https://www.springeropen.com)